Design and Implementation of Frequency Selective Radome for X-Band Applications

Cumhur Topcuoglu [1], Cihan Dogusgen Erbas [2], and Nurhan Turker Tokan [1]

[1] Department of Electronics and Communication Engineering
Yildiz Technical University, Istanbul, 34220, Turkey
f0518053@std.yildiz.edu.tr, nturker@yildiz.edu.tr

[2] Department of Electrical and Electronics Engineering
Istanbul Yeni Yuzyil University, Istanbul, 34010, Turkey
cihan.dogusgen@yeniyuzyil.edu.tr

Abstract ─ A triple layer X-band FSS is designed and its reflection and transmission characteristics are explored for normal/oblique incidence. The proposed planar FSS is confirmed by simulation and measurement results. Then, by using the X-band FSS, a novel X-band radome is designed. Its reflection and transmission characteristics are investigated for in-band and out-of band frequencies by integrating an ultra-wide band antenna. A comparison of radiation patterns at selected frequencies for cases with and without radome is examined. Adaptation of radome to the antenna is achieved without significant reduction in radiation performance at the design frequency of FSS.

Index Terms ─ Endfire radiation, frequency selective radome, unit cell, Vivaldi antenna.

I. INTRODUCTION

Frequency selective surfaces (FSSs) are planar periodic structures composed of either slot or patch elements that interact with electromagnetic waves within certain frequency band(s). They act as analogue spatial filters such that these spatial filters transmit or block waves in a specific frequency band of interest. Design process of the FSSs involves a proper choice of topology characteristics such as unit cell type and geometry, spacing between unit cells, substrate permittivity and thickness as well as presence or absence of superstrates in order to obtain the desired spectral selectivity. FSSs have a wide range of applications in electromagnetic spectrum, including radar cross section (RCS) reduction, electromagnetic interference reduction, millimeter and terahertz wave operations, antenna reflectors, quasi-optical filters, polarizers and switches [1-5].

A substantial amount of research has been conducted on the FSSs as they have unique properties and a large number of practical uses. Various FSS elements such as center connected structures (e.g., dipoles, tripoles, square spirals, Jerusalem crosses), circular, square and hexagonal loops along with numerous shapes have been intensively analyzed [6-8]. Varactor, Schottky and PIN diodes have also been embedded in active FSS design for the reconfiguration of these FSSs, while inductors are utilized as control lines [9-11]. Recently, FSSs with different unit cell geometries have been used as ground planes of microstrip patch antennas as well [12-14]. Several studies have addressed different aspects of FSSs such as mutual coupling reduction of antenna arrays, and shielding applications [15, 16]. Optimization-based design of the FSSs is also possible [17].

Another specific application of FSSs is radomes. A radome protects an antenna from outer environment with smallest effect on the radiation properties of the antenna within a frequency band of interest. Performance of a radome depends on matching its configuration and materials composition to a particular application and RF frequency range. A radome produced by curved FSSs acts as a bandpass filter that allows transmission in an operating frequency band, and reflection out of the band. It is usually difficult or impossible to control the RCS of antennas over a wide frequency range. Instead of shielding the antenna to protect it from a threat radar, which blocks the antenna operation, it is a wiser approach to cover the antenna with an FSS radome that is transparent at the operating frequency band, yet opaque at the threat radar frequency.

Although the usage of FSSs as a protective radome leads to a considerable reduction in the RCS of the enclosed antenna outside the operating band, it might affect the electrical performance of the antenna in terms of polarization purity reduction, sidelobe level increase, transmission losses, degradation in impedance matching properties, tilting of the main beam, and strong undesired electromagnetic interference. Hence, accurate radome design and production using FSSs are important.

Several studies have been reported on FSS radome design: Liu et al. [18] investigated the effect of incidence

Submitted On: March 7, 2019
Accepted On: May 23, 2019

angle and polarization on bandwidth stability for a proposed FSS structure for radomes. Angular instability was observed in the presented results. Qu et al. [19] designed a cylindrical radome based on a graphene FSS that has a tunable bandpass filtering characteristic. Sensitivity analysis for different incidence angles was not carried out in that study. Lin et al. [20, 21] developed an axi-symmetric conical FSS radome in S-band and another miniature conical thick-screen FSS in C-band, then explored the impact of these radomes on monopole antennas. Impact of the designed radomes on gain performance was unkown. Combination of different materials with FSS structures have also been of interest. In one study [22], a modified silica ceramic was developed and used in Jerusalem FSS. It was concluded that the modified substance could be used as a dielectric material for FSS radomes. Choi et al. [23] formed an X-band hybrid composite low-observable radome that consisted of a composite sandwich construction including E-glass/aramid/epoxy hybrid composite faces, a polymethacrylimide foam core and an FSS.

In this article, firstly, a triple layer X-band FSS is designed. Its reflection and transmission characteristics planar FSS is confirmed by simulation and measurement results. In the experimental verification, a waveguide measurement setup is used. Next, a novel X-band radome is designed by using a triple layer X-band FSS. Its reflection and transmission characteristics are investigated for in-band and out-of band frequencies by integrating an UWB Vivaldi as the antenna inside the radome. Design steps of the FSS radome are explained. Radiation pattern simulations at 8, 10, 12 GHz are presented. It is found that radiation properties of the antenna are not significantly affected by the coverage of the FSS radome for in-band frequencies of the FSS structure. Moreover, a flat top transmission feature is obtained. All simulations are performed with CST Microwave Studio, a commercial Finite Integration Technique (FIT) based software package. FIT is a spatial discretization technique to numerically solve electromagnetic problems in both time and frequency domain. In the process, basic topological properties of the continuous equations are preserved. The basic idea of this approach is to apply the Maxwell equations in integral form to a set of staggered grids. Thus, the accuracy and performance of a simulation in CST are heavily dependent on the quality of the mesh that describes the structure. Achieving very high mesh quality leads to more qualitative definition of the problem space. In this work, analysis process is performed in CST by using the adaptive mesh refinement to obtain better accuracy with less unknowns, especially in simulations with radome.

II. GEOMETRY OF UNIT CELL

Designed planar FSS consists of 3-layer periodic unit cells. Each unit cell has a circular metallic structure at the top and bottom layers, and a square metal part with a cross-shaped slot as the middle layer. A dielectric material fills the inter-layer volume. After a series of optimizations for the unit cell parameters and the dielectric profile, dimensions of the unit cell are obtained for X-band characteristics. Also, the dielectric material, which affects the unit cell capacitance as well as reflectance at the air-dielectric interface, is determined. Diameter of the metallic circle is denoted by D, while the arm length and width of the cross-shaped slot are expressed by L_p and W_p, respectively. Edge of the metal square in the middle layer is denoted by W. The FSS is implemented on a commercially available Rogers RO4003C high-frequency laminate with a 0.51 mm dielectric thickness and 17.5 um copper. The laminates are bonded to each other by using spray glue, which has negligible effect on electromagnetic performance [24]. The dielectric material has a relative dielectric constant of $\varepsilon_r = 3.38 \pm 0.05$, and a loss tangent of 0.0035 at 10GHz. Low dielectric loss of this laminate facilitates its use in many applications where higher operating frequencies limit the use of conventional circuit board laminates. Figure 1 shows the unit cell geometry, and Table 1 illustrates the dimensions of the unit cell. Since the array is considered as infinite in size, *y*- and *x*-boundaries are set to unit cell of the array. Floquet ports are defined at the *z*-boundaries.

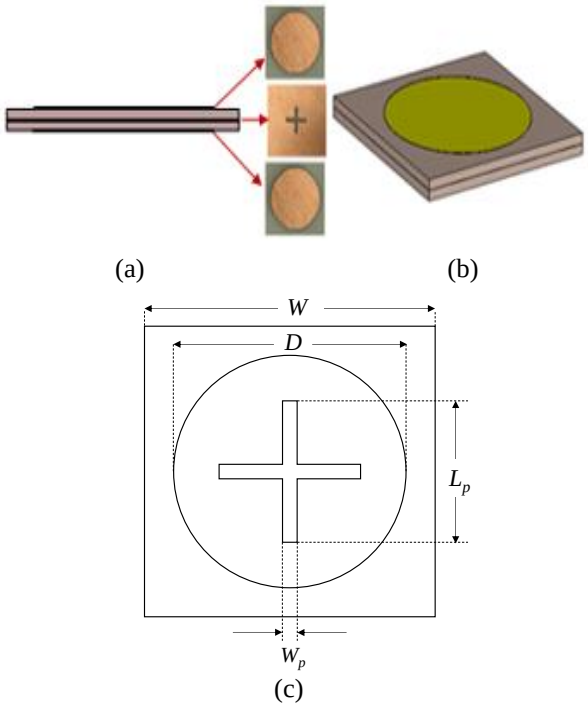

Fig. 1. Unit cell of the designed FSS: (a) side view, (b) perspective view, and (c) top view with design parameters.

Table 1: Dimensions of the unit cell for the proposed FSS

Parameter	Dimension (mm)
W	10
L_p	3.5
W_p	0.4
D	8.19

A parametric analysis is carried out to realize the identified design requirements. Our investigations (not shown here for brevity) demonstrate that top of the transmission curve occurs at smaller frequencies as W becomes larger and smaller resonant frequencies occur as L becomes larger. This is due to the increase of equivalent inductance with increasing L.

Resonant frequency of the unit cell is calculated as:

$$f = \frac{1}{2\pi\sqrt{L_U C_U}}, \quad (1)$$

where L_U and C_U are the equivalent inductance and equivalent capacitance of the unit cell, respectively. As the slot length L_p increases, the resonant frequency decreases because path length of the current increases. Lower resonant frequencies are observed as the parameter D increases. Furthermore, a flat top transmission is obtained for all D values. An increase in the dielectric constant of the dielectric material results in an increase in capacitance, which results in a decrease in the resonant frequency.

It is useful to explore the effect of incidence angle on the reflection and transmission coefficients as well. Figure 2 illustrates the incident wave that impinges on the unit cell with an angle of θ. A set of incidence angles between θ=0^O and θ=50^O with an increment of $\Delta\theta$=10^O is applied. Although resonant frequency remains unchanged with varying incidence angles, as verified by Fig. 3, the reflection coefficient becomes larger at the resonant frequency as the incidence angle increases. In order to cover a larger range of incidence angles, reflection and transmission coefficients simulated between θ=0^O and θ=90^O are depicted in Fig. 4.

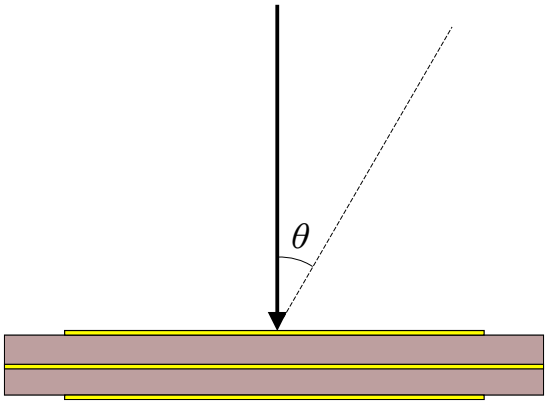

Fig. 2. Incident wave on unit cell.

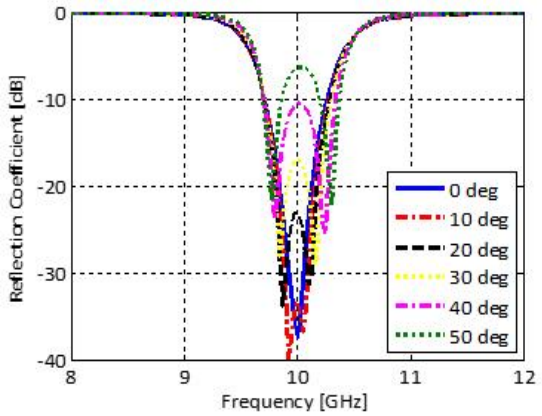

Fig. 3. Sensitivity analysis of the EM wave: reflection coefficient.

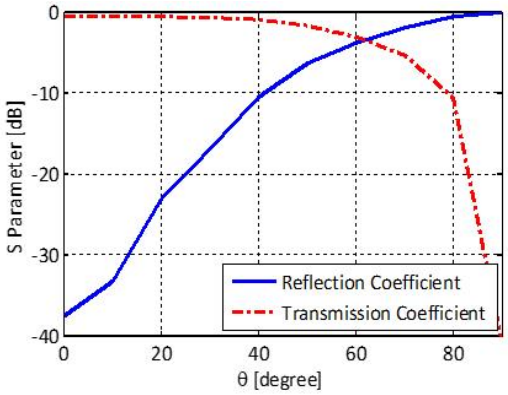

Fig. 4. Sensitivity analysis of the EM wave: comparison of reflection and transmission coefficients.

III. PLANAR FSS MEASUREMENT RESULTS

The planar FSS is theoretically infinite in extent and lies in x-y plane. Taking the two-dimensional periodicity into account, the analysis of the FSS is simplified by use of the Floquet's theorem. Practically, size of the FSS has to be limited, which is 80x80 mm (in x-y plane) consisting of 8 by 8 unit cells. Incident wave propagates in z-direction. Oblique plane waves can also impinge on the structure.

In order to verify the simulation results, the proposed FSS structure is fabricated and tested. In the fabrication process of the FSS, chemical etching technique with photolithography is employed. For the periodic structures such as FSSs, the waveguide transmission lines can be used for the measurement [25-26]. Thus, a waveguide measurement setup is used. The measurement system is illustrated in Fig. 5 (a) and Fig. 5 (b) shows the prototype of the three-layer FSS with the top array visible. The sample FSS was fitted properly within the waveguide

flanges. Part of the fabricated FSS structure and WR-90 waveguide used in the measurement are shown in Fig. 5 (b). Anritsu MS4644A 2-port vector network is used in measurements. Waveguide to coaxial adapter is used at both sides for transition. With this measurement setup, the transmission and the reflection coefficients of the FSS are measured for the dominant mode (TE_{10}). Note that due to planar behavior of the structure, the resonant frequency does not depend on the size of the FSS [27].

Figure 6 and Fig. 7 depict the measured as well as simulated results of the reflection and transmission coefficients, respectively, versus frequency. As seen from the figures, measurements and simulations are in good agreement for reflection and transmission coefficients.

The planar FSS structure might be considered as a second-order bandpass filter consisting of LC circuits [28] that yield a double resonance in the reflection coefficient curve in Fig. 6. The double resonance is observed in both the simulation and measurement results. A fast roll-off is obtained in the simulated and measured transmission coefficient curve in Fig. 7. The split at the top of the measured transmission coefficient curve could be due to measurement errors.

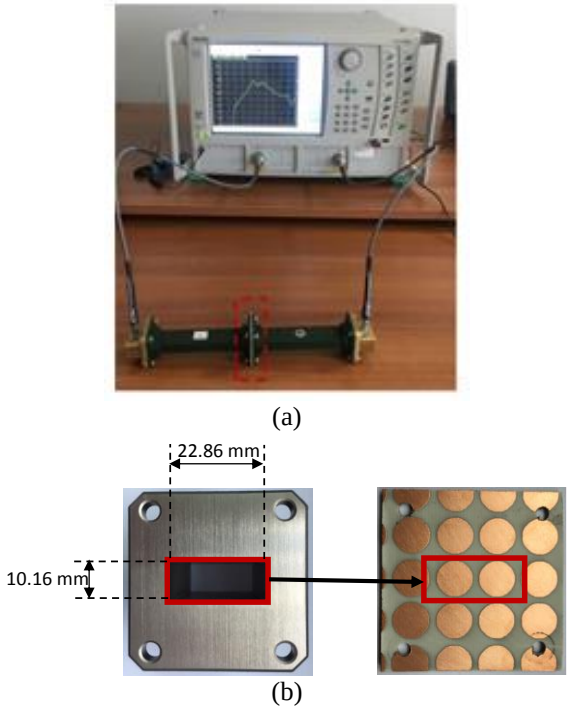

Fig. 5. Planar FSS Measurements: (a) measurement set up and (b) part of the fabricated FSS and waveguide. WR90 waveguide with 6.5 GHz cutoff frequency for dominant mode (TE_{10}) is used in the measurements. The following mode (TE_{20}) starts at 13.1 GHz.

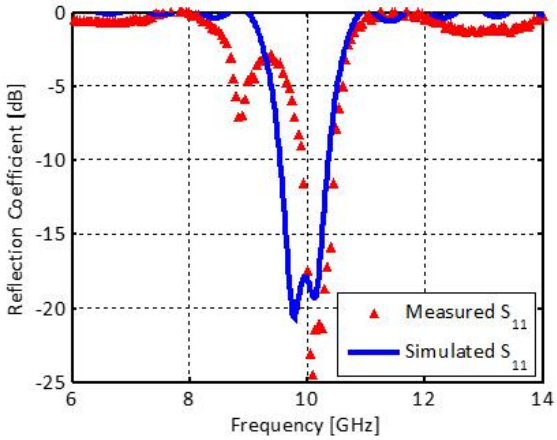

Fig. 6. Measured and simulated reflection coefficient versus frequency for the planar FSS structure.

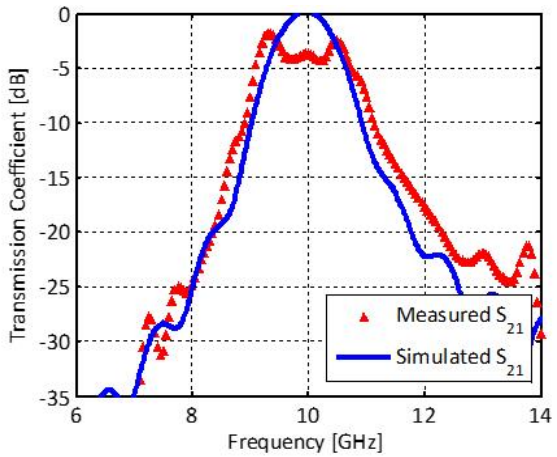

Fig. 7. Measured and simulated transmission coefficient versus frequency for the planar FSS structure.

IV. FSS RADOME DESIGN FOR ENDFIRE RADIATION

When the FSS is used in curved structures, the fundamental properties of planar FSS, namely the periodicity and the infinite extent of the surface, are lost. This makes it impossible to reduce the analysis to that of a single unit cell [29]. Therefore, electrically large curved array of FSSs have to be analyzed. The geometrical optics (GO) is commonly used for the analysis. However, multiple internal reflections are not accounted by GO.

A novel X-band radome in the shape of an extended hemispherical lens is designed by using triple layer X-band FSS. Its reflection and transmission characteristics are investigated for in-band and out-of band frequencies through simulations by integrating an available UWB Vivaldi antenna as the antenna inside the radome. Vivaldi

antenna with endfire radiation operates efficiently as a transmitter and receiver in the band of 3 GHz–15 GHz. The slot curve for the Vivaldi antenna is an exponential function expressed as:

$$S(z) = (W_{slot}/2)\, exp(az), \quad (2)$$

where a=0.165 and W_{slot}=0.25 mm. A $\lambda/4$ open circuit stub is used for wide band matching. Rogers RT/Duroid 5870 (ε_r=2.33) with a 0.51 mm dielectric thickness, and 17.5 um copper is chosen for the design. The prototype is shown in Fig. 8. The reflection behavior is measured in terms of S_{11} characteristics in Fig. 9.

The shape of the radome is synthesized as the union of a hemisphere of radius r = 60 mm (corresponds to 2λ in free space), and a cylindrical dielectric slab base with a height of h = 30mm (corresponds to 1λ in free space). These dimensions are chosen to ensure main beam inclusion of the antenna within the FSS radome for end-fire radiation. Figure 10 illustrates the designed radome, and the integrated antenna.

(a) (b)

Fig. 8. Fabricated Vivaldi antenna: (a) top view and (b) back view.

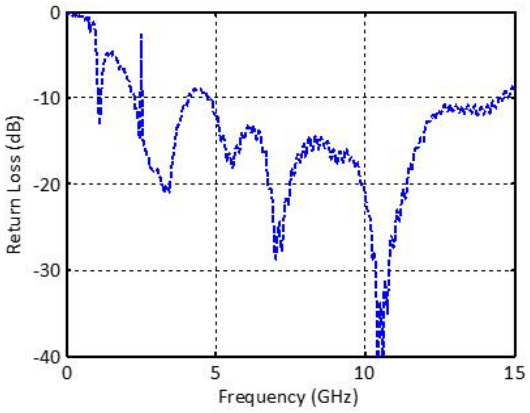

Fig. 9. Measured return loss of Vivaldi antenna.

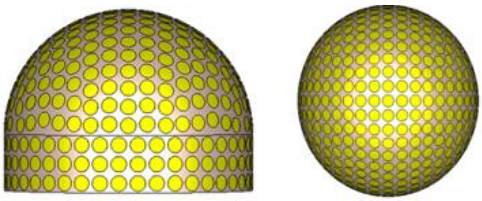

(a) (b)

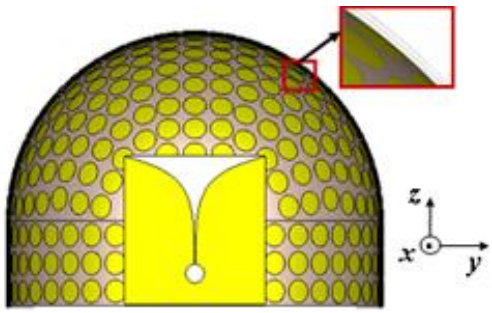

(c)

Fig. 10. FSS radome: (a) Side view, (b) top view, and (c) cut view with Vivaldi antenna.

The structure that consists of the FSS radome, located to the reactive near field region of the antenna, and Vivaldi antenna is simulated. Simulations are performed in X-band (a frequency band of 8 GHz-12 GHz), which covers the operation frequency range of the antenna. Simulated gain patterns of the antenna with and without the radome at 8 GHz, 10 GHz, and 12 GHz are given in Fig. 11. It is observed that the minimal degradation in the gain pattern occurs at 10 GHz and the direction of the main beam remains unchanged. While the gain of Vivaldi antenna at 10 GHz is 7.4 dBi, which is almost equal in E and H planes, the Vivaldi antenna with the radome has a gain of 6.7 dBi in H-plane, and 7.2 dBi in E-plane. Although E-plane results excellently match each other with/without FSS radome, H-plane patterns are degraded to some extent by the integration of FSS radome.

The gain patterns obtained with radome at 8 GHz and 12 GHz has opposite main beam direction compared to the Vivaldi antenna. This proves the no transmission and high reflection characteristics of radome for out-of-band operations.

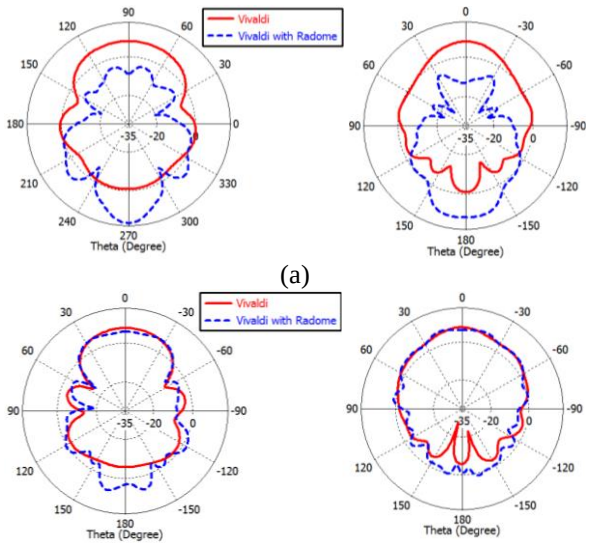

(a)

(b)

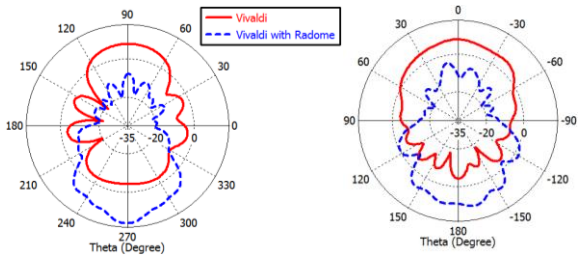

(c)

Fig. 11. Simulated gain pattern of Vivaldi antenna with FSS radome: (a) H-plane at f=8 GHz (left), E-plane at f=8 GHz (right), (b) H-plane at f=10 GHz (left), E-plane at f=10 GHz (right), and (c) H-plane at f=12 GHz (left), E-plane at f=12 GHz (right).

V. CONCLUSION

A curved radome designed through an FSS structure is presented. Unit cell geometry of the planar FSS is described in detail. The triple layer planar FSS is fabricated, assembled, and measured. Measurement and simulation results for the reflection along with transmission coefficient of the planar FSS are given. Measurement results show sufficiently good performance. FSS radome design integrated with an UWB Vivaldi antenna with endfire radiation is illustrated. Gain patterns of the Vivaldi antenna at 8 GHz, 10 GHz, and 12 GHz for the cases with and without the radome are explored. It is revealed that the gain pattern at 10 GHz yields the optimum result compared to the gain patterns at 8 GHz, and 12 GHz. Intended design of the radome is consistent with the obtained results. Compared with other previously developed radomes, current design has some advantages such as angular stability for different incidence angles, and insignificant change in gain at an optimal design frequency. A flat-top transmission feature is also achieved. It is concluded that the designed radome could be used in X-band applications. In the future, impact of the change in the radome radius on the reflection and transmission characteristics could be analyzed as the hemispherical radome approaches to a planar structure with increasing radius.

REFERENCES

[1] R. Mittra, C. H. Chan, and T. Cwik, "Techniques for analysing frequency selective surfaces – A review," *Proc. IEEE*, vol. 76, pp. 1593-1615, 1988.

[2] X. Q. Lin., T. J. Cui, Y. Fan, et al., "Frequency selective surface designed using electric resonant structures in terahertz frequency bands," *J. of Electromagnetic Waves Appl*., vol. 23, pp. 21-29, 2009.

[3] P. S. Taylor, A. C. M. Austin, E. A. Parker, et al., "Angular independent frequency selective surfaces for interference control in indoor wireless environments," *Electronics Letters*, vol. 48, pp. 61-62, 2012.

[4] G. I. Kiani, L. G. Olsson, A. Karlsson, et al., "Transmission of infrared and visible wavelengths through energy-saving glass due to etching of frequency-selective surfaces," *IET Microw. Antennas Propag*., vol. 7, pp. 955-961, 2010.

[5] R. Panwar and J. R. Lee, "Progress in frequency selective surface-based smart electromagnetic structures: A critical review," *Aerospace Science and Technology*, vol. 66, pp. 216-234, 2017.

[6] B. A. Munk, *Frequency Selective Surfaces: Theory and Design*. Wiley-Interscience, New York, 2000.

[7] M. Wang, L. Zhao, J. Wang, et al., "A low-profile miniaturized frequency selective surface with insensitive polarization," *Applied Computational Electromagnetics Society Journal*, vol. 33, no. 9, pp. 1003-1008, 2018.

[8] Y. Lin, X. Xu, Z. Dou, et al., "A novel multi-band polarization insensitive frequency selective surface based on centrosymmetric L-shaped metal strips," *Applied Computational Electromagnetics Society Journal*, vol. 30, no. 3, 2015.

[9] H. Wang, P. Kong, W. Cheng, et al., "Broadband tenability of polarization-insensitive absorber based on frequency selective surface," *Scientific Reports*, vol. 6, pp. 1-8, 2016.

[10] F. Deng, X. Xi, J. Li, et al., "A method of designing a field-controlled active frequency selective surface," *IEEE Antennas and Wireless Propagation Letters*, vol. 14, pp. 630-633, 2015.

[11] S. H. Mahmood and T. A. Denidni, "Pattern-reconfigurable antenna using a switchable frequency selective surface with improved bandwidth," *IEEE Antennas and Wireless Propagation Letters*, vol. 15, pp. 1148-1151, 2016.

[12] M. Z. Joozdani, M. K. Amirhosseini, and A. Abdolali, "Wideband radar cross-section reduction of patch array antenna with miniaturised hexagonal loop frequency selective surface," *Electronics Letters*, vol. 52, pp. 767-768, 2016.

[13] Y. Liu, Y. Hao, H. Wang, et al., "Low RCS microstrip patch antenna using frequency-selective surface and microstrip resonator," *IEEE Antennas and Wireless Propagation Letters*, vol. 14, pp. 1290-1293, 2015.

[14] Y. Jia, Y. Liu, H. Wang, et al., "Low RCS microstrip antenna using polarisation-dependent frequency selective surface," *Electronics Letters*, vol. 50, pp. 978-979, 2014.

[15] K. Yu, Y. Li, and X. Liu, "Mutual coupling reduction of a MIMO antenna array using 3-D novel meta-material structures," *Applied Computational Electromagnetics Society Journal*, vol. 33, no. 7, pp. 758-763, 2018.

[16] M. Idrees, S. Buzdar, and S. Khalid, "A miniaturized polarization independent frequency selective surface with stepped profile for shielding applications," *Applied Computational Electromagnetics Society Journal*, vol. 31, no. 5, 2016.

[17] N. F. Amini, M. Karimipour, K. Paran, et al., "Optimization of frequency selective surface with simple configuration based on comprehensive formation method," *Applied Computational Electromagnetics Society Journal*, vol. 30, no. 4, 2015.

[18] N. Liu, X. Sheng, C. Zhang, et al., "Design of frequency selective surface structure with high angular stability for radome application," *IEEE Antennas and Wireless Propagation Letters*, vol. 17, pp. 138-141, 2018.

[19] M. Qu, M. Rao, S. Li, et al., "Tunable antenna radome based on graphene frequency selective surface," *AIP Advances*, vol. 7, pp. 1-7, 2017.

[20] B. Lin, S. Du, H. Zhang, et al., "Design and simulation of frequency-selective radome together with a monopole antenna," *ACES Journal*, vol. 7, pp. 620-625, 2010.

[21] B. Lin, F. Li, Q. R. Zheng, et al., "Design and simulation of a miniature thick-screen frequency selective surface radome," *IEEE Antennas and Wireless Propagation Letters*, vol. 8, pp. 1065-1068, 2009.

[22] L. L. Zhang, J. H. Zhang, X. L. Chen, et al., "Modified silica ceramic for frequency selective surface radome," *Journal of the Ceramic Society of Japan*, vol. 123, pp. 937-941, 2015.

[23] I. Choi, D. Lee, and D. G. Lee, "Hybrid composite low-observable radome composed of E-glass/ aramid/epoxy composite sandwich construction and frequency selective surface," *Composite Structures*, vol. 117, pp. 98-104, 2014.

[24] R. Orr, V. Fusco, D. Zelenchuk, G. Goussetis, et al., "Circular polarization frequency selective surface operating in ku and ka band," *IEEE Trans. Antennas Propag*., vol. 63, pp. 5194-5197, 2015.

[25] S. Cimen, "Novel closely spaced planar dual-band frequency-selective surface," *IET Microw. Antennas Propag.*, vol. 7, pp. 894-899, 2013.

[26] F. Bayatpur and K. Sarabandi, "Tuning performance of metamaterialbased frequency selective surfaces," *IEEE Trans. Antennas Propag.*, vol. 57, pp. 590-592, 2009.

[27] Z. Sipus, M. Bosiljevac, and S. Skokic, "Analysis of curved frequency selective surfaces," *Report*, p. 48, 2007.

[28] M. N. Jazi, M. R. Chaharmir, J. Shaker, and A. R. Sebak, "Broadband transmitarray antenna design using polarization-insensitive frequency selective surfaces," *IEEE Trans. Antennas Propag*., 64, vol. 1, pp. 99-108, 2016.

[29] Z. Sipus, M. Bosiljevac, and S. Skokic, "Analysis of curved frequency selective surfaces," *The Second European Conference on Antennas and Propagation (EuCAP 2007)*, Edinburgh, UK, pp. 1-5, 2007.